Experimental and theoretical study of acceptor activation and transport properties in *p*-type $Al_xGa_{1-x}N$/GaN superlattices

I. D. Goepfert and E. F. Schubert
Department of Electrical and Computer Engineering, Boston University, Boston, Massachusetts 02215

A. Osinsky and P. E. Norris
NZ Applied Technologies, Woburn, Massachusetts 01801

N. N. Faleev
Electrical Engineering Department, Texas Tech University, Lubbock, Texas 79409

(Received 29 November 1999; accepted for publication 10 May 2000)

Experimental and theoretical results of Mg-doped superlattices consisting of uniformly doped $Al_xGa_{1-x}N$, and GaN layers are presented. Acceptor activation energies of 70 and 58 meV are obtained for superlattice structures with an Al mole fraction of $x=0.10$ and 0.20 in the barrier layers, respectively. These energies are significantly lower than the activation energy measured for Mg-doped bulk GaN. At room temperature, the doped superlattices have free-hole concentrations of $2\times10^{18}\,\mathrm{cm}^{-3}$ and $4\times10^{18}\,\mathrm{cm}^{-3}$ for $x=0.10$ and 0.20, respectively. The increase in hole concentration with Al content of the superlattice is consistent with theory. The room temperature conductivity measured for the superlattice structures is 0.27 S/cm and 0.64 S/cm for an Al mole fraction of $x=0.10$ and 0.20, respectively. X-ray rocking curve data indicate excellent structural properties of the superlattices. We discuss the origin of the enhanced doping, including the role of the superlattice and piezoelectric effects. The transport properties of the superlattice normal and parallel to the superlattice planes are analyzed. In particular, the transition from a nonuniform to a uniform current distribution (current crowding) occurring in the vicinity of contacts is presented. This analysis provides a transition length of a few microns required to obtain a uniform current distribution within the superlattice structure. © *2000 American Institute of Physics.*
[S0021-8979(00)03816-0]

INTRODUCTION

Efficient *n*- and *p*-type doping of III-nitride semiconductors is imperative for the development of wideband gap electronic and optoelectronic devices. Silicon (Si) is the donor of choice for GaN with an experimental activation energy between 10–25 meV.[1] At room temperature nearly all of the donors are ionized. By contrast, the large activation energy of magnesium (Mg) of 150 to 250 meV[2–4] results in a low acceptor ionization probability, with only a few percent activation at room temperature. Other acceptors such as beryllium (Be) and calcium (Ca) also have large activation energies of 150[5] and 169 meV,[6] respectively. The low acceptor activation in *p*-type GaN results in large parasitic resistances, high operating voltages, and high specific contact resistances, which adversely affect the performance of electronic and optoelectronic devices.

Recently, it has been theoretically and experimentally demonstrated that doped $Al_xGa_{1-x}N$/GaN superlattice structures increase the free-hole concentration as compared to bulk *p*-type GaN.[7–12] Doped superlattices are doped ternary compound semiconductor structures with a modulated chemical composition. The modulation of the chemical composition leads to a variation of the valence band energy and to a reduction of the effective acceptor activation energy. Acceptors in the GaN layers of the superlattice must be ionized by thermal excitation. However, acceptors in the $Al_xGa_{1-x}N$ barriers are ionized more easily because these acceptors are energetically close to the GaN valence band edge. It has been shown that the modulation of the valence band edge results in a strong enhancement of the free-hole concentration. The possible increase in free-hole concentration in $Al_xGa_{1-x}N$/GaN superlattices over bulk GaN was shown to be one order of magnitude. In addition, piezoelectric effects have been proposed to cause the doping enhancement in $Al_xGa_{1-x}N$/GaN doped superlattice structures.[11,12] Theoretical and experimental results on doped $Al_xGa_{1-x}N$/GaN superlattice structures will be discussed in this article including the acceptor activation, hole concentration, conductivity, mobilities, and current crowding.

ACCEPTORS IN GaN AND $Al_xGa_{1-x}N$

The simple hydrogen atom model modified for the dielectric constant and effective mass of the semiconductor predicts an acceptor ionization energy of

$$E_a=\frac{1}{\varepsilon_r^2}\frac{m_h^*}{m_0}\frac{e^4 m_0}{2(4\pi\varepsilon_0\hbar)^2}=\frac{1}{\varepsilon_r^2}\frac{m_h^*}{m_0}\,13.6\,\mathrm{eV}, \tag{1}$$

where $m_h^*=0.8\,m_0$ is the GaN heavy hole effective mass and $\varepsilon_r=9.0$ is the GaN relative permittivity.[2] Equation (1) yields a GaN acceptor ionization energy of 134 meV. For AlN with $m_h^*=0.8\,m_0$[13] and $\varepsilon_r=8.5$,[2] an ionization energy of 151 meV is inferred from Eq. (1). Consequently, the hydrogenic model predicts an increase of 13% of the acceptor activation

 © 2000 American Institute of Physics

energy in AlN when compared with GaN. For an Al mole fraction of $x=25\%$, the acceptor ionization energy is expected to be 138 meV, only slightly higher than the GaN acceptor activation energy.

The effective Bohr radius is given by

$$r_B^* = \frac{4\pi\varepsilon_r\varepsilon_0\hbar^2}{m_h^* e^2} = \frac{\varepsilon_r}{m_h^*/m_0} 0.053\,\text{nm}, \tag{2}$$

which yields 0.60 nm for GaN and 0.56 nm for AIN. It has been pointed out that for small radii, on the order of the lattice constant, the effective dielectric constant used in the hydrogenic impurity model should be lower than the bulk dielectric constant.[14] This would increase the calculated acceptor activation energy, and bring it in closer agreement with experimental values of approximately 200 meV.

Theoretical calculations based on effective-mass theory for degenerate hole bands, reported by Mireles and Ulloa,[15] determined ionization energies of 197–245 meV and 465–758 meV for Mg acceptors in wurtzite GaN and AIN, respectively. For an Al content of $x=25\%$ in $Al_xGa_{1-x}N$, the ionization energy will range between 264 and 373 meV, assuming a linear extrapolation.

We have recently reported an ionization energy of 200 meV for Mg in epitaxial bulk GaN.[16] This value is in good agreement with other values reported in the literature which range between 150 and 250 meV.

To date, there are few publications with experimental results concerning the electronic properties of doped AIN. This is due to the insulating nature of AIN which has a band gap energy of 6.2 eV. Several studies have been performed on the ionization energy of Mg in $Al_xGaN_{1-x}N$ with Al mole fractions less than 30%. Tanaka *et al.*[17] measured an ionization energy for Mg in $Al_{0.08}GaN_{0.92}N$ of 192 meV and for bulk GaN of 157 meV.

Katsuragawa and co-workers[18] showed that as the Al content is increased in bulk $Al_xGa_{1-x}N$ from $x=0.00$ to $x=0.33$, the hole concentration decreases monotonically. Using the parameters $\varepsilon_r=9.0-0.5\ x$ for the relative permittivity of $Al_xGa_{1-x}N$[19] and $m_h^*=0.8\,m_0$ for the effective hole mass,[20] the hydrogenic model does not predict a significant deepening of the acceptor level in $Al_xGa_{1-x}N$ for $x\leqslant 0.20$. This is consistent with the experimental results of Katsuragawa *et al.*,[18] who showed that the activation energy does not change markedly for Al content $x\leqslant 0.30$. Recently, however, Stutzmann and co-workers[21] reported an increase of the Mg activation energy from $E_a=170\,\text{meV}$ for GaN to $E_a=360\,\text{meV}$ for $Al_{0.27}Ga_{0.73}N$. Considering the range of experimental data reported for the acceptor activation energy in $Al_xGa_{1-x}N$, we use the deepening predicted by the hydrogenic model for the acceptor activation energy in $Al_xGa_{1-x}N$.

DOPED $Al_xGa_{1-x}N$/GaN SUPERLATTICES

A schematic of the band diagram of a uniformly doped, composition-modulated semiconductor is illustrated in Fig. 1(a). We assume that the period of the superlattice is much larger than the acceptor Bohr radius in either the GaN or the $Al_xGa_{1-x}N$. Since $r_B^*=0.60\,\text{nm}$ for GaN and $r_B^*=0.57\,\text{nm}$ for AIN, the acceptor energy levels in the wells and barriers will be tied to the band edges in the respective materials. For a superlattice period $z_p=20\,\text{nm}$, as used in this study, this condition is indeed fulfilled. Figure 1(b) schematically shows the free-hole concentration and the ionized acceptor concentration. The figure indicates that free carriers collect in the GaN wells, whereas ionized acceptors are located mostly in the $Al_xGa_{1-x}N$ barriers. As will be discussed later, the free carrier and ionized impurity distribution can change when taking into account polarization effects.

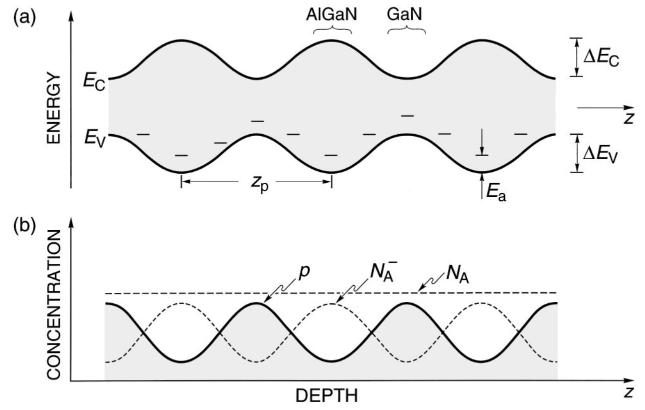

FIG. 1. (a) Band diagram of a semiconductor superlattice with a modulated chemical composition that induces a conduction band edge and valence band edge modulation. E_C, E_F, and E_V are the conduction band energy, the Fermi energy, and the valence band energy, respectively. The dashed line represents the acceptor state in the energy gap. The period of the superlattice is z_p. (b) Schematic of the doping concentration N_A and hole concentration p of a composition modulated semiconductor.

High electrical activation of deep acceptors is achieved if the acceptor levels in the barriers are energetically close or even above the valence band states in the wells. This condition may be expressed as

$$\Delta E_V - E_a \geqslant E_{oh} + (E_F - E_{oh}) + E_{\text{dipole}}, \tag{3}$$

where E_{oh} is the quantized subband energy in the GaN valence band well relative to the valence band edge, $(E_F - E_{oh})$ is the band filling of the quantized valence subband states, and E_{dipole} is the energy due to the transfer of holes from acceptor states in the $Al_xGa_{1-x}N$ barriers to the GaN wells. The dipole energy can be calculated by a double integration of Poisson's equation

$$E_{\text{dipole}} = -\frac{e^2}{\varepsilon}\int_0^{z_p/2}\int_0^z [p(z') - N_A^-(z')]dz'\,dz, \tag{4}$$

where z_p is the period of the superlattice structure. The period of the structure is chosen small enough to make band bending effects negligible, $E_{\text{dipole}} \ll \Delta E_v$. However, the period of the structure is chosen sufficiently large to make confinement effects negligible, i.e., $E_{oh} \ll \Delta E_v$. For our structures, the GaN well thickness is approximately 10 nm so that $E_{oh}=5\,\text{meV}$. Thus, the relation $E_{oh} \ll \Delta E_v$ is satisfied.

Doped superlattices are modeled using an SGI Origin 2000 computer and Silvaco's ATLAS device simulation software. A two-period superlattice structure of $Al_xGa_{1-x}N$ with x varied between zero and 30 percent is numerically simulated. The superlattice structure is composed of a periodic

$Al_xGa_{1-x}N/GaN$ superlattice with thickness of 10 nm/10 nm, respectively. The carrier concentration versus depth is determined by numerically solving Poisson's equation

$$\frac{d^2\Phi}{dz^2} = -\frac{e}{\varepsilon}(p - N_A^-) = -\frac{e}{\varepsilon}\left(\int_{-\infty}^{E_V} \frac{m_h^*}{\pi^2\hbar^3} \frac{\sqrt{2m_h^*(E_v - E)}}{1+\exp\left(\frac{E_F - E}{kT}\right)} dE - \frac{N_A}{1+g_A\exp\left(\frac{E_A - E_F}{kT}\right)}\right), \tag{5}$$

where Φ is the electrostatic potential, e is the elementary charge, ε is the permittivity, p is the hole concentration, and N_A^- is the ionized acceptor concentration. In Eq. (5b) the first term in brackets is the hole concentration p expressed in integral form: m_h^* is the effective hole mass, E_v is the valence band energy, $\hbar$ is Planck's constant, E_a is the acceptor energy, E_F is the Fermi energy, k is Boltzmann's constant, and T is absolute temperature. The second term in brackets of Eq. (5b) expresses the ionized acceptor concentration N_A^- as the product of the total acceptor concentration N_A and the probability of ionization. The degeneracy factor is $g_A = 2$. A uniform doping profile of $N_A = 1\times10^{18}\,\text{cm}^{-3}$ with an activation energy of $E_a = 200\,\text{meV}$ in the GaN and $Al_xGa_{1-x}N$ layers is assumed.

The valence band discontinuity occurring at $GaN/Al_xGa_{1-x}N$ interfaces is modeled with the following equation:

$$\Delta E_V = \tfrac{1}{3}\{[xE_{g,\text{AlN}} + (1-x)E_{g,\text{GaN}} - x(1-x)E_{\text{bowing}}] - E_{g,\text{GaN}}\}, \tag{6}$$

where x is the Al mole fraction in $Al_xGa_{1-x}N$, $E_{g,\text{AlN}} = 6.2\,\text{eV}$ is the band gap of AlN at 300 K, $E_{g,\text{GaN}} = 3.4\,\text{eV}$ is the band gap of GaN at 300 K, and E_{bowing} is the bowing parameter. The term in the braces represents the band gap difference between GaN and $Al_xGa_{1-x}N$. The factor 1/3 preceding the brackets on the right-hand side of Eq. (6) is the percentage of the band gap difference allocated to the valence band.[22] The measured bowing parameter, as reported in the literature, varies between $-0.8 < E_{\text{bowing}} < 1.3\,\text{eV}$. Critical for determining the bowing parameter is the correct assessment of the Al concentration in $Al_xGa_{1-x}N/GaN$ heterostructures. Koide *et al.*[23] used both x-ray diffractometry and electron probe microanalysis to determine the Al mole fraction in their samples. They determined a bowing parameter $E_{\text{bowing}} = 1.0 \pm 0.3\,\text{eV}$. Recently, Angerer *et al.*[24] have determined a bowing parameter of $E_{\text{bowing}} = 1.3\,\text{eV}$. Angerer *et al.* used both x-ray diffraction and elastic recoil detection analysis to determine the Al mole fraction in their samples. The values 1.0–1.3 eV are now well accepted for the bowing parameters of the gap of $Al_xGa_{1-x}N$.

Figure 2 depicts the acceptor concentration, the effective hole concentration of the superlattice structure, the calculated hole concentration of bulk GaN, and the calculated hole concentration of the superlattice. The effective hole concentration of the superlattice structure is defined as the arithmetic average of the free carrier concentration over one period of the superlattice. Note that the effective hole concentration is one order of magnitude larger than the free hole concentration in bulk Mg-doped GaN.

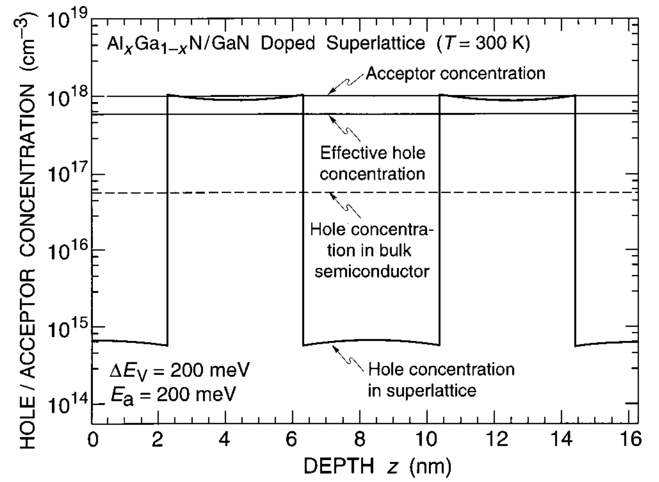

FIG. 2. Numerical simulation of the hole concentration in a uniformly doped superlattice structure with a modulated valence band edge. The acceptor concentration $N_A = 1\times10^{18}\,\text{cm}^{-3}$, the effective hole concentration $p_{\text{eff}} = 5\times10^{17}\,\text{cm}^{-3}$ (defined as the arithmetic average over one period of the superlattice), the hole concentration in bulk p-type semiconductor $p = 5.5\times10^{16}\,\text{cm}^{-3}$, and the hole concentration in the superlattice are depicted. The acceptor concentration for the bulk semiconductor is $N_A = 1\times10^{18}\,\text{cm}^{-3}$.

Figure 3(a) shows the calculated modulation of the valence band edge versus depth into the superlattice structure, Fig. 3(b) shows the calculated free-hole concentration versus depth of the superlattice structure, and Fig. 3(c) shows the calculated ionized acceptor concentration versus depth of the

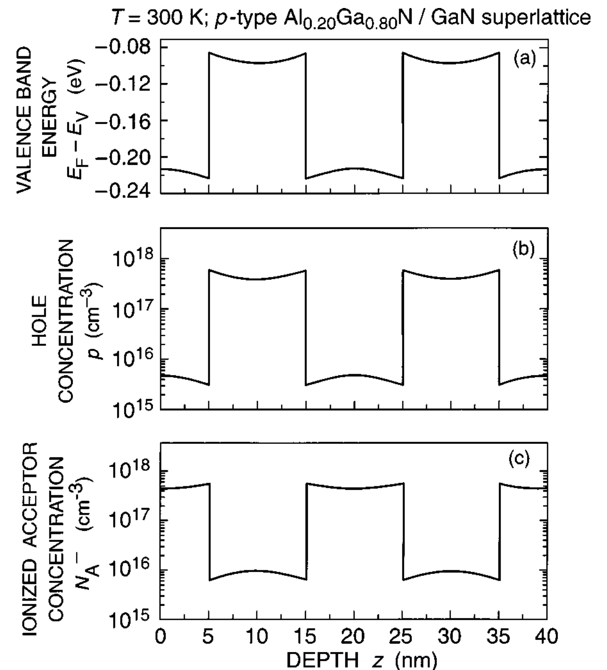

FIG. 3. Composite of calculated results of a two-period superlattice structure doped with $N_A = 1\times10^{18}\,\text{cm}^{-3}$ (a) the valence band energy E_V, (b) the hole concentration p, (c) the ionized acceptor concentration N_A^-.

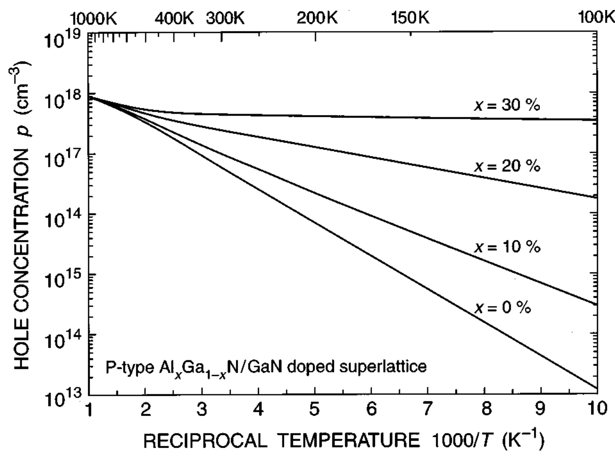

FIG. 4. Calculated hole concentration versus reciprocal temperature for p-type $Al_xGa_{1-x}N$/GaN doped superlattices with Al mole fractions of $x=0.00$, 0.10, 0.20, and 0.30.

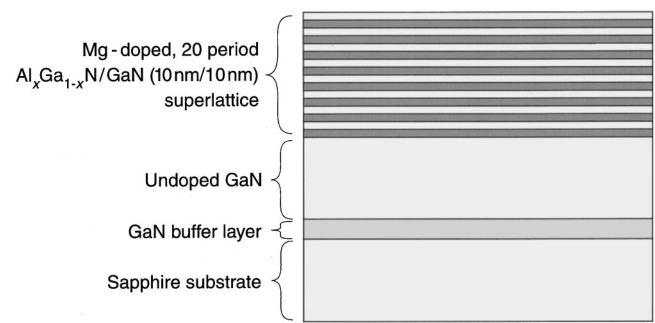

FIG. 5. A schematic of the 20-period, Mg-doped, $Al_xGa_{1-x}N$/GaN superlattice structure on which electronic measurements were performed is illustrated. The superlattice was grown on top of an undoped GaN layer. In the initial growth phase a GaN buffer layer was deposited on the sapphire substrate.

superlattice structure. Note that in the $Al_xGa_{1-x}N$ barriers the hole concentration is much lower that in the GaN wells, while concurrently, the ionized acceptor concentration in the $Al_xGa_{1-x}N$ barriers is much higher than in the GaN wells. This modulation of carrier concentration and ionized acceptor concentration due to the modulation of the valence band energy is the underlying physical process that enhances the free-hole concentration in doped superlattice structures.

The calculated effective carrier concentration versus inverse temperature for various superlattice structures is depicted in Fig. 4. In Fig. 4 there are four curves, each representing a superlattice structure with a different Al content in the $Al_xGa_{1-x}N$ barrier, illustrating the effective carrier concentration versus the inverse of temperature. Examination of each of the four curves shows that the effective carrier concentration is enhanced for a given temperature until the temperature reaches the freeze-out/saturation transition temperature of approximately 700 K. Note that the slopes of p versus $1/T$ in the freeze-out regime represent the effective ionization energy of the acceptor. The slopes indicate that the acceptor activation energy decreases with increasing Al mole fraction in the superlattice barriers.

Recently, it was proposed that spontaneous polarization and piezoelectric polarization plays a role in enhancing the hole concentration in doped superlattice structures.[12] Spontaneous and piezoelectric polarization effects can create high internal electric fields that tilt the band edge with respect to the Fermi level. As a result, some acceptors are moved *below* the Fermi level while other acceptors are moved *above* the Fermi level. Thus, polarization effects create an additional band modulation that may increase the ionized acceptor concentration over what is achieved with only the modulation of the valence band edge induced by the superlattice structure. Due to the complex atomic structure of the interface of wurtzite heterostructures, it is difficult to predict the exact magnitude of spontaneous and piezoelectric polarization effects.[25]

However, we have calculated the free-hole concentration in the superlattices taking into account polarization effects. We find that, although the band diagram changes significantly when taking into account polarization effects, the overall hole concentration is not enhanced significantly over the values calculated without polarization effects. Note that a factor of 10 enhancement is already obtained without polarization effects.

DOPED SUPERLATTICES—EXPERIMENTAL RESULTS

The structural characteristics and electronic properties of $Al_xGa_{1-x}N$/GaN doped superlattice structures grown by MBE are analyzed. The superlattices consist of 20 periods of equally thick $Al_xGa_{1-x}N$ barriers (10 nm) and GaN wells (10 nm). Figure 5 is a schematic diagram of the samples on which electronic measurements are conducted. The $Al_xGa_{1-x}N$ and GaN layers are uniformly doped with Mg at a level of $N_{Mg}\approx 10^{19}\,cm^{-3}$. The Al mole fractions of the two different doped superlattices are $x=0.10$ and 0.20, respectively.

Superlattice crystal quality, Al mole fraction, and periodicity are evaluated by a high-resolution x-ray diffraction technique. A Philips ''*X*-pert''diffractometer equipped with a (220)-oriented Ge Bartels-type monochromator, and threefold Ge (220) analyzer crystal was used for the measurements. The measurements were performed with $CuK_{\alpha1}$ radiation.

The double-crystal rocking curves for two 20-period p-type $Al_xGa_{1-x}N$/GaN doped superlattices are shown in Fig. 6. The two satellite peaks that correspond to the -1, $+1$ orders of reflection confirm that both superlattice structures have a periodic variation of the chemical composition and good parallelism of the interfaces between the GaN and the $Al_xGa_{1-x}N$ layers of the superlattice. The parameters derived from the relative position of the -1, $+1$, and 0 reflections give superlattice periods of 18.5 and 19.5 nm for the structures with an Al content of $x=10\%$ and 20% in the $Al_xGa_{1-x}N$ barriers, respectively. These data are in good agreement with the intended superlattice period of 20 nm. Inspection of curves 1 and 2 in Fig. 6 reveals that second-order reflections are not observed in the rocking curves. The suppression of the second order of reflection is known to occur if the well to barrier layer thickness ratio ($Al_xGa_{1-x}N$ to GaN ratio in our case) is close to 1. The absence of the

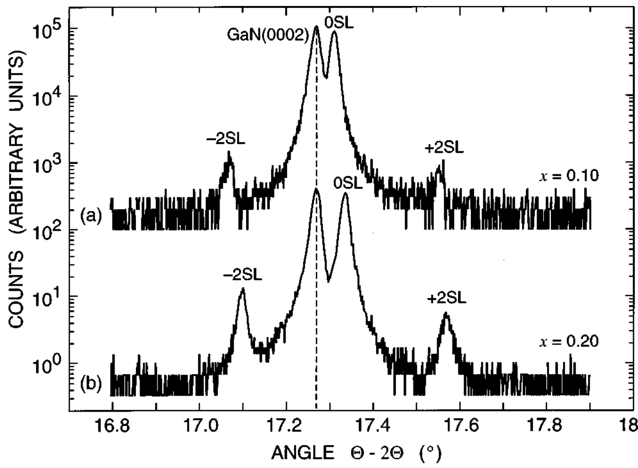

FIG. 6. Double-crystal rocking curves for two 20-period $Al_xGa_{1-x}N$/GaN doped superlattices with (a) $x=0.1$, and (b) $x=0.20$.

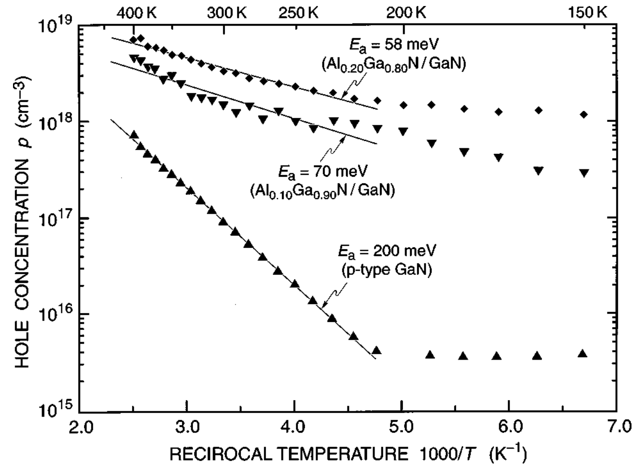

FIG. 7. Hole concentration versus reciprocal temperature for Mg-doped $Al_xGa_{1-x}N$/GaN superlattice samples with Al mole fraction in the barriers of $x=0.10$ and 0.20. Also shown is a uniformly Mg-doped bulk GaN sample with an acceptor activation energy of 200 meV.

second-order reflections confirms that the GaN well thickness is very similar to the $Al_xGa_{1-x}N$ barrier thickness in the $Al_xGa_{1-x}N$/GaN superlattices studied here.

The average Al mole fraction x in the superlattices can be derived from the zero-order reflection position. Using the zero-order position, we determine average Al mole fractions of 5.25% and 9% for the two superlattice structures considered here. The average Al mole fraction is in good agreement with the values set during the growth of the samples. Taking into account that the GaN well and $Al_xGa_{1-x}N$ barrier layer thicknesses are equal, the Al concentration in the $Al_xGa_{1-x}N$ barrier layers are 10.5% and 18% for the two superlattice structures, close to the nominal values of 10% and 20%, respectively.

The somewhat asymmetric shape of the superlattice reflections displayed in curve 2 of Fig. 6 indicates that there may be a slight Al composition gradient in the $Al_xGa_{1-x}N$ barrier layers of the superlattice structure with Al mole fraction of $x=18\%$. The Al composition in the $Al_xGa_{1-x}N$ barriers may gradually increase towards the surface of the structure.

Hall-effect measurements in the van der Pauw configuration were conducted on Mg-doped $Al_xGa_{1-x}N$/GaN superlattice samples. Photolithographically defined, 85 nm thick Ni contacts were deposited by electron-beam evaporation. All samples display ohmic (linear) $I-V$ characteristics. The samples were cooled in a Cryo Industries liquid nitrogen cryostat. Hall-effect measurements were made between 150–400 K with 10 K intervals using a magnetic induction of 0.5 T.

Figure 7 shows the free-hole concentration versus reciprocal temperature. The hole concentration displays an exponential dependence versus $1/T$ for temperatures in the range 220–400 K. The natural logarithm of the carrier concentration versus reciprocal temperature is fit with a least-squares regression algorithm. The activation energy is then determined by the relation

$$\ln p \propto -E_a/(kT), \tag{7}$$

where E_a is the acceptor activation energy, k is Boltzmann's constant, and T is the absolute temperature. The measured activation energies for the superlattices with $x=0.10$ and $x=0.20$ are 58 and 70 meV, respectively. This result clearly shows that doped $Al_xGa_{1-x}N$/GaN superlattice structures have a lower activation energy than Mg-doped bulk GaN.

At room temperature, the carrier concentration of the doped superlattice structures are $2\times10^{18}\,cm^{-3}$ and $4\times10^{18}\,cm^{-3}$ for an Al mole fraction $x=0.10$ and 0.20, respectively. The sample with an Al content of 20% has a factor of 2 larger carrier concentration than the sample with an Al content of 10%. Thus, the free-hole concentration increases with an increase in Al mole fraction in the barriers of the superlattices. This increase is consistent with theory. It should be noted that most free carriers reside in the GaN layers. Assuming that the carrier concentration in the barriers is much smaller,[7] the actual free-carrier concentration in the GaN layers of the superlattice is $8\times10^{18}\,cm^{-3}$, which is the highest free-hole concentration reported in GaN.

Katsuragawa and co-workers[18] showed that as the Al content is *increased* in bulk $Al_xGa_{1-x}N$ from $x=0.00$ to $x=0.33$, the free-hole concentration *decreases* monotonically. Tanaka and co-workers[26] reported that the Mg activation energy increases from 157 meV in GaN to 192 meV in $Al_{0.08}GaN_{0.92}N$. In contrast, Fig. 7 indicates that doped superlattice structures have *smaller* activation energies and *larger* carrier concentrations as the Al mole fraction in the barriers is increased.

The conductivity versus temperature for the two superlattice structures is depicted in Fig. 8. At room temperature, the conductivity for the superlattice with $x=20\%$ has a conductivity almost a factor of 3 greater than for the superlattice with $x=10\%$ Al. Note that the results shown in Fig. 8 are among the highest p-type conductivities achieved in a III-nitride semiconductor containing Al.

Figure 9 depicts the mobility versus temperature for the doped superlattice samples. Note that for an increase in Al content, the mobility does not change. The mobilities of the doped superlattice structures increase monotonically with

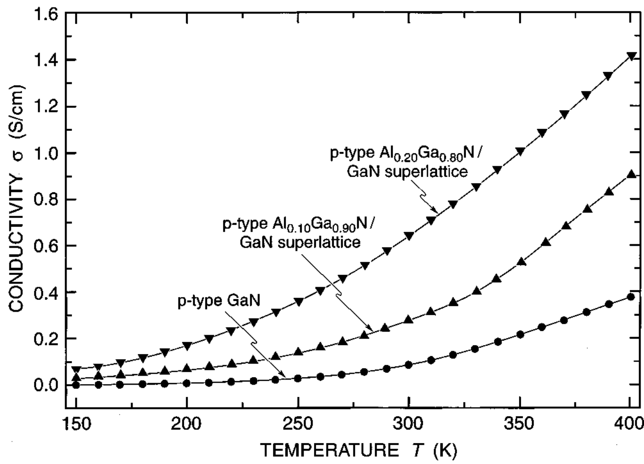

FIG. 8. Conductivity versus temperature for p-type $Al_xGa_{1-x}N/GaN$ doped superlattices and bulk p-type GaN.

temperature by more than a factor of 3 in the temperature range 150–400 K. This is in contrast to bulk p-type GaN, which exhibits a decrease in mobility as the temperature increases beyond 200 K. Due to the temperature dependence of the mobility, conductivity data without carrier concentrations[12,27] may result in an overestimation of the acceptor activation energy.

UNIFORMITY OF TRANSPORT AND CURRENT CROWDING EFFECTS IN DOPED SUPERLATTICES

The transport properties of superlattices are inherently anisotropic. To determine the impact of the superlattice structure on the current distribution, the superlattice is modeled in terms of a network of resistors perpendicular and parallel to the superlattice planes. The superlattice is assumed to consist of 10 nm GaN and wells and 10 nm $Al_xGa_{1-x}N$ barriers. Superlattices with 10 and 20 periods are numerically simulated. The Al mole fraction is varied between 0% and 30%. Figure 10 illustrates a schematic of a two-period $Al_xGa_{1-x}N/GaN$ superlattice structure represented by a network of resistors perpendicular and parallel to

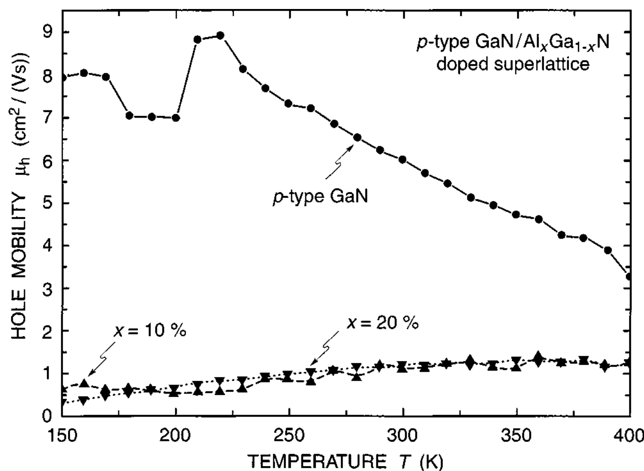

FIG. 9. Mobility versus temperature for p-type $Al_xGa_{1-x}N/GaN$ doped superlattices and bulk p-type GaN.

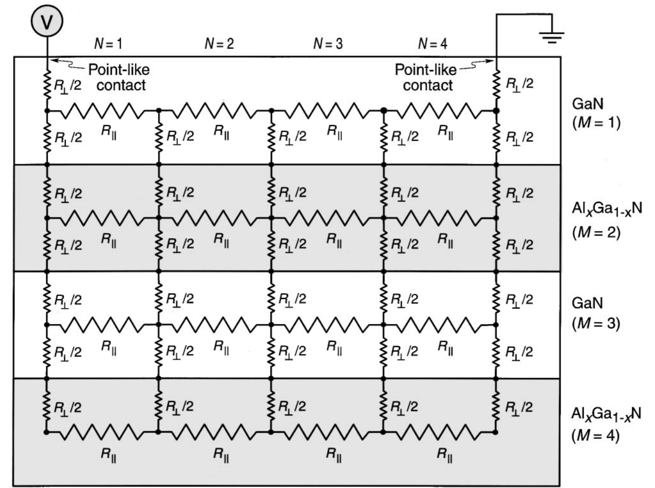

FIG. 10. Schematic of a two-period $Al_xGa_{1-x}N/GaN$ superlattice structure represented by a network of resistors perpendicular and parallel to the plane of the superlattice structure.

the plane of the superlattice structure. A *simplified* schematic of the two period $Al_xGa_{1-x}N/GaN$ superlattice structure is depicted in Fig. 11. In this simplified circuit diagram, the parallel resistors ($R_{\parallel}$) in the $Al_xGa_{1-x}N$ layers have been neglected since $R_{\parallel}(Al_xGa_{1-x}N) \gg R_{\parallel}(GaN)$. Also, the perpendicular resistors ($R_{\perp}$) in the GaN layers have been neglected since $R_{\perp}(Al_xGa_{1-x}N) \gg R_{\perp}(GaN)$. The resistors represent either GaN or $Al_xGa_{1-x}N$ layers and are ''bricks'' (parallelepipeds) with a length of 100 nm, a height of 10 nm, and a depth of 1 μm. The depth and length directions are *parallel* to the superlattice planes and the height direction is *perpendicular* to the superlattice planes. The two parallel directions are physically equivalent. Table I displays the numerical values of the parallel and perpendicular resistors used in the calculation. A distance of 100 μm is assumed between two point-like contacts capping the superlattice structure, as indicated in Fig. 10. The resistors R_i, voltage drops across the resistors V_i, potential at the nodes ϕ_i, and

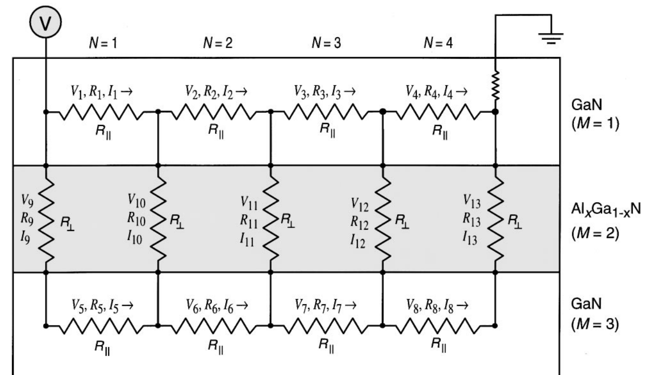

FIG. 11. Simplified schematic of a two-period $Al_xGa_{1-x}N/GaN$ superlattice structure represented by a network of resistors. The parallel resistors in the $Al_xGa_{1-x}N$ layers have been neglected since $R_{\parallel}(Al_xGa_{1-x}N) \gg R_{\parallel}(GaN)$. The perpendicular resistors in the GaN layers have been neglected since $R_{\perp}(Al_xGa_{1-x}N) \gg R_{\perp}(GaN)$. The resistors R_i, voltage drops across the resistors V_i, potential at the nodes ϕ_i, and current I_i are enumerated in the same manner as the large-scale simulation.

TABLE I. Calculated resistor values for $x=0.10$, 0.20, and 0.30 used to model the doped $Al_xGa_{1-x}N$/GaN doped superlattice structures with a network of resistors.

Superlattice structure	Superlattice resistors $R_\perp$	Superlattice resistors $R_\parallel$
$x=0.10$		
$p_{GaN}=2\times10^{17}$ cm^{-3} $p_{Al_xGa_{1-x}N}=2\times10^{16}$ cm^{-3}	0.36 MΩ	3.4 MΩ
$x=0.20$		
$p_{GaN}=5\times10^{17}$ cm^{-3} $p_{Al_xGa_{1-x}N}=4\times10^{15}$ cm^{-3}	1.6 MΩ	1.3 MΩ
$x=0.30$		
$p_{GaN}=9\times10^{17}$ cm^{-3} $p_{Al_xGa_{1-x}N}=5\times10^{14}$ cm^{-3}	12 MΩ	0.72MΩ

currents I_i indicated in Fig. 11 are enumerated in the same manner as the large-scale simulation which has several hundred resistors.

The voltage drop across each resistor in the network may be represented in matrix notation as[28]

$$\mathbf{V}=\mathbf{V}_{\text{applied}}-\mathbf{A}\phi, \tag{8}$$

where $\mathbf{V}$ is the vector of voltage drops across the resistors, $\mathbf{V}_{\text{applied}}$ is the vector of voltage sources, $\mathbf{A}$ is the edge-node incidence matrix[28] (also referred to as the connectivity or topology matrix), and ϕ is the vector of unknown voltages at each node. Ohm's law and Kirchhoff's current law are employed to find the unknown currents I_i and voltages ϕ_i and are expressed as follows:

$$\mathbf{I}=\mathbf{C}(\mathbf{V}_{\text{applied}}-\mathbf{A}\phi), \tag{9}$$

$$\mathbf{A}^T\mathbf{I}=0, \tag{10}$$

where $\mathbf{C}$ is the conductance matrix and $\mathbf{A}^T$ is the transpose of the edge-node incidence matrix $\mathbf{A}$.

Figure 12 shows the simulated current flow parallel to the superlattice plane in a 20-period 10 nm/10 nm $Al_{0.20}Ga_{0.80}N$/GaN superlattice structure. The current distribution at the contact ranges over more than two orders of magnitude between the first (top) GaN well and the 20th (bottom) GaN well. At a distance of approximately 2 μm from the contact, the horizontal current flow in the superlattice structure is uniformly distributed over all layers of the superlattice structure. We define the current to be uniformly distributed, if the currents flowing in *any* of the GaN layers is within 10% of the *average* current flowing in the GaN layers.

Figure 13 shows the current perpendicular to the plane of the superlattice for a 20-period 10 nm/10 nm $Al_{0.20}Ga_{0.80}N$/GaN superlattice structure. Note the perpendicular current changes by 13 orders of magnitude over a distance of 20 μm. This indicates that the current flowing perpendicular to the superlattice structure becomes insignificantly small at a small distance from the contact.

Figure 14 shows the numerically calculated distance (solid lines and solid symbols) where uniform current flow is attained parallel to the plane of the superlattice structure. The solid lines represent the calculated results of the current $\mathbf{I}$ in

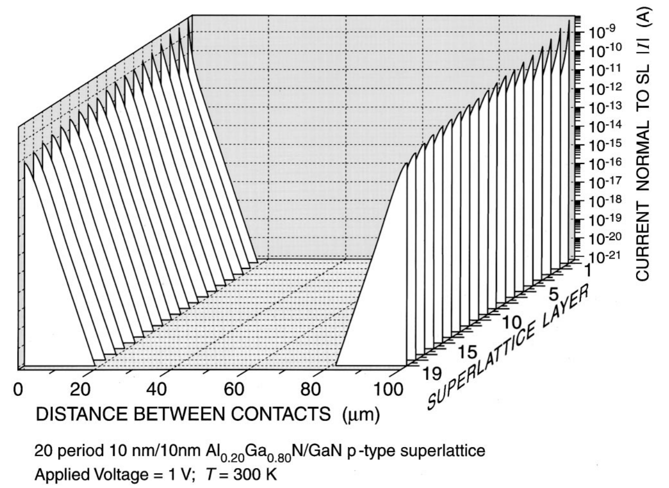

FIG. 13. Numerical simulation of the absolute value of the current flowing perpendicular to the superlattice plane in a 20-period 10 nm/10 nm $Al_{0.20}Ga_{0.80}N$/GaN superlattice structure with $N_A=1\times10^{18}$ cm^{-3}.

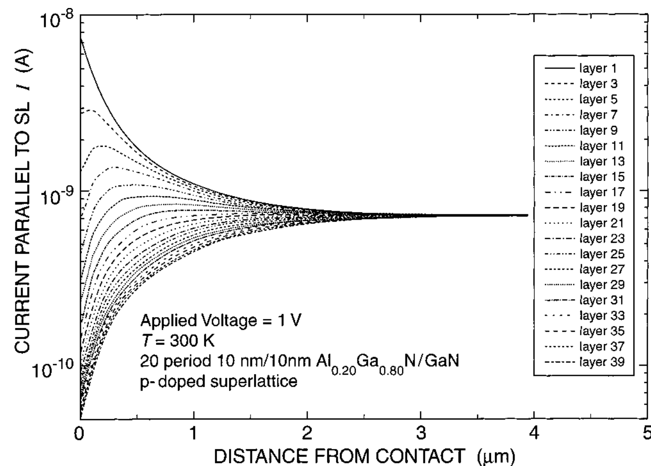

FIG. 12. Numerical simulation of current flowing parallel to the superlattice plane in a 20-period 10 nm/10 nm $Al_{0.20}Ga_{0.80}N$/GaN superlattice structure with $N_A=1\times10^{18}$ cm^{-3}.

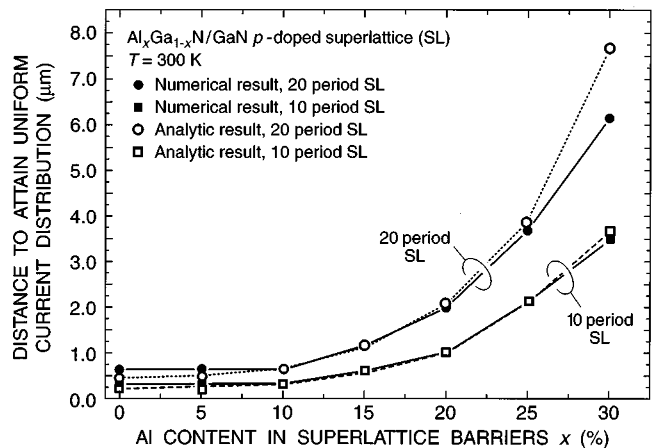

FIG. 14. Theoretical and numerical results of convergence of uniform current flow parallel to the superlattice plane.

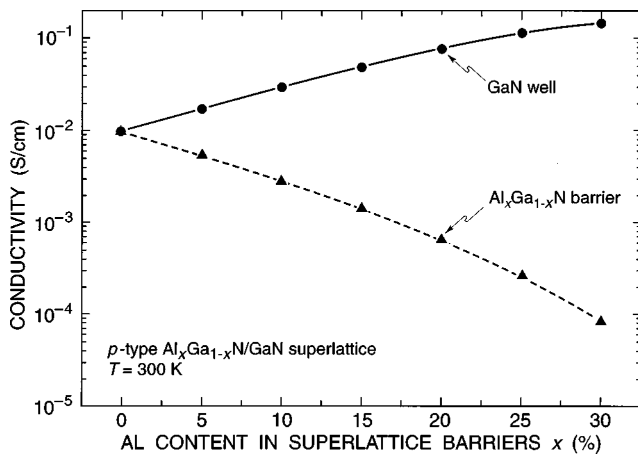

FIG. 15. Conductivity versus Al mole fraction x for the $Al_xGa_{1-x}N$ barriers and GaN wells of a superlattice structure.

Eq. (9) where the current parallel to the superlattice is uniform within 10% of the average current parallel to the superlattice.

We next derive an analytic expression for the length required to attain uniform current distribution. The condition for uniform parallel current distribution may be translated into length with the following general expression:

$$L=f(R_{\parallel},R_{\perp}N,M), \tag{11}$$

where L is the length at which uniform current flow is attained. This length is a function of the number of perpendicular resistors M and the number of parallel resistors N. We assume that the current distribution among all layers of the superlattice is uniform if the overall *perpendicular resistance* is equal to the *parallel resistance*, i.e.,

$$\frac{1}{N}(MR_{\perp})=\frac{1}{M}(NR_{\parallel}), \tag{12}$$

where N is the number of resistor ''columns'' and M is the number of resistor ''rows,'' as illustrated in Fig. 10. Solving Eq. (12) for N and multiplying the result by the geometrical length of the resistor (100 nm) yields the distance L where the current parallel to the superlattice plane becomes uniform across all layers of the superlattice. The distance L may then be expressed as follows:

$$\begin{aligned} L&=N\times(\text{length of resistor})\\ &=M\sqrt{R_{\perp}/R_{\parallel}}\times(\text{length of resistor}). \end{aligned} \tag{13}$$

This result, for a 10- and 20-period superlattice, is shown in Fig. 14 (dashed lines and open symbols). The results depicted in Fig. 14 illustrate that the *numerically* calculated and *analytically* calculated lengths for uniform current distribution are in good agreement and that this transition length in the superlattice structure is just a few microns long.

Figure 15 shows the conductivity for the $Al_xGa_{1-x}N$ barriers and the GaN wells as a function of Al mole fraction x which was used to calculate the above-mentioned transition length. Note that the conductivity in the GaN wells increases by about one order of magnitude, while the conductivity in the barriers drops by about two orders of magnitude as x increases from 0% to 30%. The change in conductivity is caused primarily by the large difference in the carrier concentration between the two layers. As the Al mole fraction of the barrier layers increases, $R_{\perp}$ increases and so does the distance from the contact at which uniform current distribution is established. This property of doped superlattices needs to be taken into account when designing devices such as bipolar transistors which require a low access resistance of the p-type base layer.

CONCLUSION

In conclusion, theoretical and experimental results on the electronic properties of Mg-doped superlattices consisting of uniformly doped $Al_xGa_{1-x}N$ and GaN layers are analyzed. Hall-effect measurements reveal acceptor activation energies of 70 and 58 meV for superlattice structures with Al mole fractions of $x=10\%$ and 20% in the barrier layers, respectively. These energies are substantially lower than the activation energy measured for Mg-doped bulk GaN. At room temperature, the doped superlattices have free-hole concentrations of $2\times10^{18}\,\text{cm}^{-3}$ and $4\times10^{18}\,\text{cm}^{-3}$ for $x=10\%$ and 20%, respectively. The increase in hole concentration with Al mole fraction of the superlattices is consistent with theory. The room temperature conductivity measured for the superlattice structures are 0.27 S/cm and 0.64 S/cm for an Al mole fraction of $x=10\%$ and 20%, respectively. X-ray rocking curve data display the excellent parallelism of the superlattice structures. We discuss the origin of the enhanced doping, including the effect of the superlattice and polarization effects. The transport properties parallel and perpendicular to the plane of the superlattice are analyzed. In particular, the transition from a nonuniform to a uniform current distribution occurring in the vicinity of contacts is presented. This analysis provides a lateral transition length of a few microns required to obtain a uniform current distribution within the superlattice structure.

ACKNOWLEDGMENTS

The work at Boston University was supported in part by the ONR (Dr. C. E. C. Wood) and by the NSF (Dr. R. P. Khosla). The work at NZ Applied Technologies was supported by the NSF (Dr. D. Gorman).

[1] W. Grieshaber, E. F. Schubert, I. D. Goepfert, R. F. Karlicek, Jr., M. J. Schurman, and C. Tran, J. Appl. Phys. **80**, 4615 (1996).
[2] S. Strite and H. Morkoc, J. Vac. Sci. Technol. B **10**, 1237 (1992).
[3] H. Nakayama, P. Hacke, M. R. H. Khan, T. Detchprohm, K. Hiramatsu, and N. Sawaki, Jpn. J. Appl. Phys. **35**, L282 (1996).
[4] S. Fischer, C. Wetzel, E. E. Haller, and B. K. Meyer, Appl. Phys. Lett. **67**, 1298 (1995).
[5] C. Ronning, E. P. Carlson, D. B. Thomson, and R. F. Davis, Appl. Phys. Lett. **73**, 1622 (1998).
[6] J. W. Lee, S. J. Pearton, J. C. Zolper, and R. A. Stall, Appl. Phys. Lett. **68**, 2102 (1996).
[7] E. F. Schubert, W. Grieshaber, and I. D. Goepfert, Appl. Phys. Lett. **69**, 3737 (1996).
[8] E. F. Schubert, ''Semiconductor having enhanced acceptor activation,'' U.S. Patent 5,932,899 (1999).
[9] I. D. Goepfert, E. F. Schubert, A. Osinsky, and P. E. Norris, Electron. Lett. **35**, 1109 (1999).
[10] P. Kozodoy, Y. Smorchkova, M. Hansen, and H. Xing, Appl. Phys. Lett. **75**, 2444 (1999).

[11] P. Kozodoy, M. Hansen, S. P. DenBaars, and U. Mishra, Appl. Phys. Lett. **74**, 3681 (1999).
[12] P. Kozodoy, M. Hansen, S. P. Denbaars, and U. K. Mishra, Appl. Phys. Lett. **74**, 3681 (1999).
[13] M. N. Yoder, ''Semiconductors for the visible and ultra violet'' in ''Integrated Optics and Optoelectronics,'' edited by K.-K. Wong and M. Razeghi, Proceedings of SPIE **CR45**, 105 (1993).
[14] E. F. Schubert, *Doping in III–V Semiconductors* (Cambridge University Press, Cambridge, England, 1993).
[15] F. Mireles and S. E. Ulloa, Phys. Rev. B **58**, 3879 (1998).
[16] I. D. Goepfert, E. F. Schubert, and A. Osinsky, unpublished (1999).
[17] T. Tanaka, A. Watanabe, H. Amano, Y. Kobayashi, I. Akasaki, S. Yamazaki, and M. Koile, Appl. Phys. Lett. **65**, 593 (1994).
[18] M. Katsuragawa, S. Sota, M. Komori, C. Anbe, T. Takeuchi, H. Sakai, H. Amano, and I. Akasaki, J. Cryst. Growth **189/190**, 528 (1998).
[19] We use $\varepsilon_r = 9.0$ and $\varepsilon_r = 8.5$ for the relative dielectric constant for GaN and AlN, respectively. These values are compiled by Strite and Morkoc; see Ref. 2.
[20] The experimental effective hole mass in $Al_xGa_{1-x}N$ is unknown at this time, although Katsuragawa *et al.* in Ref. 14 reported no significant change in the activation energy of Mg in $Al_xGa_{1-x}N$, indicating no significant change in the hole mass. See, for instance, Gil, *Group III Nitride Semiconductor Compounds* (Clarendon, Oxford, 1998).
[21] M. Stutzmann, O. Ambacher, A. Cros, M. S. Brandt, H. Angerer, R. Dimitrov, N. Reinacher, T. Metzger, R. Hopler, D. Brunner, F. Freudenberg, R. Handschuh, and Ch. Deger, Mater. Sci. Eng., B **50**, 212 (1997).
[22] E. A. Albanesi, W. R. L. Lambrecht, and B. Segal, Mater. Res. Soc. Symp. Proc. **339**, 607 (1994).
[23] Y. Koide, H. Itoh, R. H. Khan, K. Hiramatu, N. Sawaki, and I. Akasaki, J. Appl. Phys. **61**, 4540 (1987).
[24] H. Angerer, D. Brunner, F. Freudenberg, O. Ambacher, M. Stutzmann, R. Höpler, T. Metzger, E. Born, G. Dollinger, A. Bergmaier, S. Karsch, and H. J. Kömer, Appl. Phys. Lett. **71**, 1504 (1997).
[25] O. Ambacher, J. Smart, J. R. Shealy, N. G. Weimann, K. Chu, M. Murphy, W. J. Schaff, L. G. Eastman, R. Dimitrov, L. Wittmer, M. Stuzmann, W. Rieger, and J. Hilsenbeck, J. Appl. Phys. **85**, 3222 (1999).
[26] T. Tanaka, A. Watanabe, H. Amano, Y. Kobayasi, I. Akasaki, S. Yamazaki, and M. Koike, Appl. Phys. Lett. **65**, 593 (1994).
[27] A. Saxler, W. C. Mitchel, P. Kung, and M. Razeghi, Appl. Phys. Lett. **74**, 2023 (1999).
[28] G. Strang, *Introduction to Applied Mathematics* (Wellesley-Cambridge, Wellesley, MA, 1986).